Astronomy & Astrophysics manuscript no. Be˙Chara˙V25
February 10, 2011

Kinematics and geometrical study of the Be stars 48 Per and ψ Per with the VEGA/CHARA interferometer

O. Delaa[1,3], Ph. Stee[1], A. Meilland[2], J. Zorec[3], D. Mourard[1], Ph. Bério[1], D. Bonneau[1],O. Chesneau[1], J.M. Clausse[1], P. Cruzalebes[1], K. Perraut[4], A. Marcotto[1], A. Roussel[1], A. Spang[1], H. McAlister[5,6], T. ten Brummelaar[6], J. Sturmann[6], L. Sturmann[6], N. Turner[6], C. Farrington[6], and P.J. Goldfinger[6]

[1] Lab. H. Fizeau, CNRS UMR 6525, Univ. de Nice-Sophia Antipolis, Obs. de la Côte d'Azur, Avenue Copernic, 06130 Grasse, France
[2] Max Planck Intitut fur Radioastronomie, Auf dem Hugel 69, 53121 Bonn, Germany
[3] Institut d'Astrophysique de Paris, UMR 7095 du CNRS, Université Pierre & Marie Curie, 98bis bd. Arago, 75014 Paris, France
[4] UJF/CNRS LAOG, 414, rue de la Piscine, Domaine Universitaire 38400 Saint-Martin dHres, France
[5] Georgia State University, P.O. Box 3969, Atlanta GA 30302-3969, USA
[6] CHARA Array, Mount Wilson Observatory, 91023 Mount Wilson CA, USA

Received; accepted

ABSTRACT

Context. Five different physical processes might be responsible for the formation of decretion disks around Be stars: fast rotation of the star, stellar pulsations, binarity, stellar winds and magnetic fields. Our observations indicate that fast rotation seems to produce a disk in Keplerian rotation, at least in the specific case of the two stars observed. We do not know if this observational result is a generality or not.
Aims. We measure the size, orientation, shape, and kinematics of the disks around 2 Be stars, namely 48 Per and ψ Per.
Methods. We used the VEGA/CHARA interferometer with a spectral resolution of 5000 to obtain spectrally dispersed visibility modulus and phases within the Hα emission line.
Results. We were able to estimate the disk extension in the continuum and in the Hα line, as well as flattening, for both stars. Both stars rotate at nearly a critical rotation, but while the disk of 48 Per seems to be in Keplerian rotation, our preliminary data suggest that the disk of ψ Per is possibly faster than Keplerian, similarly to what has been found for κ CMa with observations carried out in the near-IR. However, more data is needed to confirm the fast rotation of the disk.
Conclusions. Assuming a simple uniform disk model for the stellar photosphere in the continuum and a Gaussian brightness distribution in the line emission region, we obtain a ratio of the disk diameter over the photospheric diameter of 8 48 Per and 11 for and ψ Per. We also found that the major axis of 48 Per is parallel to the polarization angle and not perpendicular to it as previously observed for many Be stars, including ψ Per. This might be due to the optical thickness of the disk, which is also responsible for the incoherent scattering of a non negligible part of the Hα line emission. To our knowledge, this is the first time that this effect has been measured in a Be star.

Key words. Techniques: high angular resolution – Techniques: interferometric – Stars: emission-line, Be – Stars: winds, outflows – Stars: individual (48 Per, ψ Per) – Stars: circumstellar matter

1. Introduction

Classical Be stars are main sequence B-type stars with high rotational velocities surrounded by a flattened rotating circumstellar environment. This circumstellar environment produces strong emission lines and is also responsible for an infrared excess, due mainly to free-free and free-bound transitions (Gehrz et al. 1974). These two outstanding characteristics define what is called the "Be phenomenon". The geometry and structure of the envelopes around Be stars have been intensively studied, and there is clear evidence that these environments are axisymmetric and flattened (Dougherty & Taylor 1992; Hanuschik 1996; Quirrenbach et al. 1997; Stee 2003; Kervella & Domiciano de Souza 2006; Tycner et al. 2008) with a very low expansion velocity (Poeckert & Marlborough 1978b,a; Waters 1986; Waters et al. 1987; Waters & Marlborough 1992; Meilland et al. 2007a). Studies of accretion disks show that disks in hydrodynamic equilibrium and in Keplerian rotation should be very thin, assuming that their vertical scale height is governed by gas pressure alone. For a disk to be thicker, either additional mechanisms have to be invoked or we must assume that the disk might not be in equilibrium (Bjorkman & Carciofi 2004). Alternatively, hydrostatic equilibrium might not be determined only by gas pressure but also by magnetic fields (Arias et al. 2006; Zorec et al. 2007), resulting in an increase in their vertical scale height.

Send offprint requests to: Omar.Delaa@obs-azur.fr

Many questions remain unsolved regarding the actual structure of circumstellar envelopes around Be stars. To understand this structure we need to understand the dominant mass ejection mechanisms from the central star, as well as to resolve which of the different scenarios for redistribution of this matter in the stellar environment may be correct. The study of the geometry and kinematics of these envelopes can be used to restrain theories of the various physical processes involved in the production of circumstellar disks. Unfortunately, this cannot be done using single telescopes since the typical angular extent of these disks is of a few mas. Consequently, long baseline interferometry combining high spatial and spectral resolution is the most suitable technique for probing Be star circumstellar environments lead to new insights into Be star physics.

In the following, we present the first interferometric CHARA/VEGA observations of two Be stars: 48 Per and ψ Per. In Sect. 2 we discuss the two targets and focus our attention on the interferometric data already obtained. In Sect. 3 we briefly introduce the CHARA/VEGA instrument, our observations, and the data reduction process. The reduced data and first analysis using geometrical models is presented in Sect. 4, whereas more advanced modeling is presented in Sect. 5. Finally, results are discussed in Sect. 6 and, Sect. 7 concludes this study.

2. The targets

2.1. 48 Per

The source 48 Persei (HD 25940, B3 Ve) was shown to have double emission line profiles many years ago (Burbidge & Burbidge 1953) and there has been a great deal of controversy concerning the inclination angle of this star, the total mass contained in the disk and the mass loss rate. Originally classified by Slettebak (1949) as a pole-on star Ruusalepp (1982), by computing line profiles for a sample of stars with a range of orientations and angular velocities, found that the inclination of 48 Per ranges in fact between 35 deg and 40°. More recently, using the Mk III interferometer equipped with a 100 Å spectral filter centered on the Hα line combined with spectropolarimetric data from the University of Wisconsins Pine Bluff Observatory (PBO), Quirrenbach et al. (1997) obtained a diameter of 2.77 ± 0.56 mas for the circumstellar environment of 48 Per and found that it was nearly spherical. They also estimated its inclination angle and confirmed the pole-on classification given by Slettebak (1949). Using the method of Barnes & Evans (1976) and Barnes et al. (1976), they derived a photospheric diameter of 0.34 mas with an error of about 20 %. From theoretical calculations with the SIMECA code in the Brγ continuum, Stee (2003) obtained estimates of the mass loss, opening angle and mass of the circumstellar disk of this star. He found a mass loss rate $\dot{M} = 6.31 \times 10^{-8}$ M$_\odot$ yr^{-1}, in good agreement with the mass-loss rates found by Waters et al. (1987): $\dot{M} = 1.3 \times 10^{-8}$ M$_\odot$ yr^{-1}. However, Stee (2003) also obtained a disk opening angle of about 2°, whereas Waters et al. (1987) inferred an angle of 28.4°. Stee (2003) also calculated the total mass of the disk to be $M = 11.2 \times 10^{-10}$ M$_\odot$, a value three times higher than the one given by Rinehart et al. (1999), i.e. $M = 3.7 \times 10^{-10}$ M$_\odot$. Grundstrom & Gies (2006) demonstrate that there are monotonic relationships between the emission-line equivalent width and the ratio of the angular half-width at half-maximum of the projected disk major axis to the radius of the star. They showed that their predicted Hα disk radii are consistent with the one directly obtained by long baseline interferometry. They used these relationships to derive the ratio $R_{\rm d}/R_\star$, where $R_{\rm d}$ is the disk radius and $R_\star$ is the stellar radius. For 48 Per, this ratio is equal to 7.4 ± 1.1, which is in good agreement with the value directly obtained by interferometry: 7.2 ± 1.5 Quirrenbach et al. (1997). They also estimated a disk inclination angle of 31° by comparing the predicted ratio of the projected minor-to-major axis with the observed one.

2.2. ψ Per

The source ψ Per (HD 22192, HR 1087) is classified as a B4IIIe Underhill et al. (1979) with a diameter of 4.7 ± 0.3 $R_\odot$ Bohm-Vitense (1989). It was listed by Campbell (1895) among stars with Hα line emission. Since then, ψ Per has been extensively studied using spectroscopy and photometry, but it has had fewer interferometric measurements than the well known Be star γ Cas.

Taylor et al. (1987) carried out a VLA radio survey at NRAO of a small sample of Be stars with strong excess emission in the IRAS bands, but the only star detected with radio emission at 4.86 GHz was ψ Per, at a level of 0.23 ± 0.04 mJy. After combining this radio flux with IR (JHKL bands) and far-UV IUE spectroscopic data, these authors concluded that the circumstellar environment in ψ Per was not spherical, but instead has a disk like structure. This result was confirmed by Dougherty & Taylor (1992) with the VLA, who were able to fully resolve the radio emission at 15 GHz of ψ Per along its major axis. They found it has a spatial extension of 111 ± 16 mas and a position angle for the major axis of 158° ± 10. However, the star could not be resolved along its minor axis at an upper limit of 3σ representing 68 mas. Dougherty & Taylor (1992) concluded that their observations confirm the equatorial enhanced circumstellar plasma distribution as the source of the Be star emission (Struve 1931).

Ten years later, Quirrenbach et al. (1997) calculated the diameter of the Hα emitting region using the Mk III optical interferometer. Applying the method by Barnes & Evans (1976) and Barnes et al. (1976) of photospheric diameter determination, they derived a diameter of 0.35 ± 0.07 mas. With a Gaussian model of brightness distribution in the disk, they also measured a diameter of 3.26 ± 0.23 mas for the circumstellar envelope using an Hα filter with a bandwidth of 100 Å. This diameter is roughly 30 times smaller than in the radio emission, but the position angle for the minor axis of $-33° \pm 11°$ is in good agreement with the determination in the radio frequency. Interestingly, it implies that there is no misalignment between the larger scale envelope out to $\sim 100\, R_\star$ where the radio emission occurs, and both the inner zone of the disk where the polarization originates and the intermediate region where the Hα emission is produced. They also obtained an axial ratio of 0.47 ± 0.11 and concluded that the circumstellar environment of ψ Per was clearly elongated in the visible, even though

Table 1. Log of observations. See Fig 1 for the orientation of baselines B1, B2, B3, and B4

Object	Date (UTC)	Telescopes	Projected Baseline Length (m)	Position Angle (deg)	r_0 (cm)	Detectors	Calibrators
ψ Per	07/10/2008 11h33	S1S2 (B1)	32.35	-20.92	9	Blue and Red	HD 12303
	08/10/2008 06h52	S1S2 (B2)	32,54	18,38	8	Blue and Red	HD 12303
	09/10/2008 07h48	W1W2 (B3)	98,32	128,6	9	Red only	HD 12303
	09/10/2008 10h43	W1W2 (B4)	107,82	93,23	10	Red only	HD 12303
48 Per	07/10/2008 12h48	S1S2 (B1)	31,84	-26,65	10	Blue and Red	HD 18411
	08/10/2008 07h29	S1S2 (B2)	32,65	17,88	9	Blue and Red	HD 18411
	09/10/2008 07h03	W1W2 (B3)	90,29	147,88	10	Blue and Red	HD 18411
	09/10/2008 11h22	W1W2 (B4)	107,7	91,9	8	Blue and Red	HD 18411

they were not able to resolve the minor axis in the radio wavelengths, probably owing to the nearly edge-on projection of the disk. Using the SIMECA code, Stee (2003) derive an estimate of the ψ Per mass-loss rate $\dot{M} = 5.0 \times 10^{-8}$ $M_\odot$ yr^{-1}, the mass of its disk $M = 110^{-9}$ $M_\odot$, and the opening angle of the disk $\sim 1°$, which are consistent with similar determinations by Waters et al. (1987) and Rinehart et al. (1999). All determinations by Stee (2003) were made using the Brγ continuum emission and interferometric data.

3. Observations and data reduction

The VEGA instrument (Mourard et al. 2009) at the CHARA array (ten Brummelaar et al. 2005) is located on the Mount Wilson Observatory just north of Los Angeles in California, USA. It operates in the visible domain and benefits from both a high-resolution spectrograph and a polarimeter. The spectrograph is designed to sample the visible band from 0.45 to 0.85 μm and is equipped with two photon-counting detectors that simultaneously observe in two different spectral bands.

3.1. Observations

Observations of 48 Per and ψ Per CHARA/VEGA were carried out using both the Red and Blue detectors, centered on 656 nm (Hα line) and around 486 nm, respectively, in October 2008. We used the medium spectrograph resolution of R = 5000. Each observation was performed using only two out of six one-meter telescopes of the CHARA array. Details of the observations are given in Table 1, and the *(u,v)* plane coverage is presented in Fig 1.

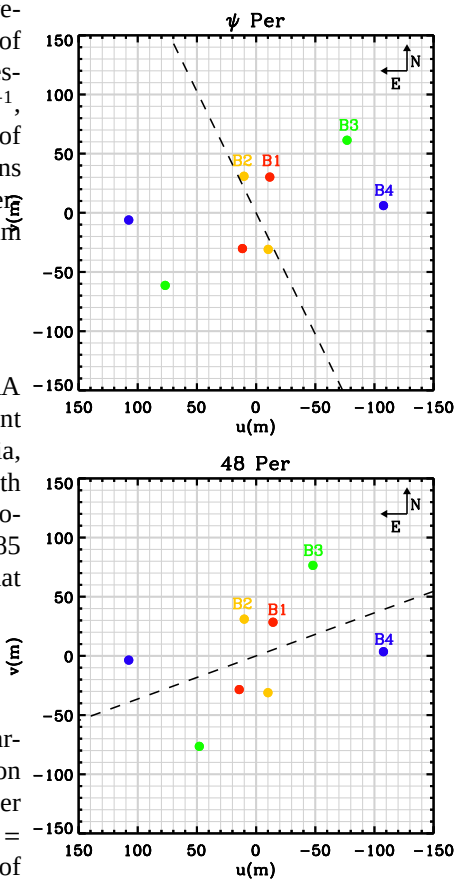

Fig. 1. .(u,v) plane coverage of the observed Be stars. The dashed lines represents the polarization angle measured by Yudin (2001).

3.2. Data reduction

The data reduction was done using the software developed by the VEGA group and described in Mourard et al. (2009). This software offers two data reduction modes, the first one is based on the spectral density analysis of the fringe signal in a single optical band, and the second one on the cross-spectral analysis scheme. In the spectral density mode, we obtain one measurement, i.e. the squared visibility averaged over a spectral band centered on a given wavelength λ_1. With the cross-spectral analysis mode, we obtain the visibility modulus V(λ) and the differential phase $\phi_{\rm diff}$ within many narrow channels, each a few angstroms in width, covering a large spectral band. For each channel, we measured the product $V(\lambda_1)\times V(\lambda_2)$ and $\phi_{\rm diff}(\lambda_2)$. The same processing is done for the calibrators HD 18411 & HD 12303, whose angular diameters θ_{LD} (0.41 ± 0.03 mas, m_v = 4.677 mag for HD 18411 and 0.26 ± 0.02 mas, m_v = 4.992 mag for HD 12303) were estimated using the SearchCal software (Bonneau et al. 2006) from the Jean-Marie Mariotti Center[1]. The visibilities in the Hα line were measured using pass bands of $\delta\lambda$ = 2.4 nm for ψ Per and $\delta\lambda$ = 1.75 nm for 48 Per, which cover the width of these lines in each case (see Fig. 3). The

[1] http://www.jmmc.fr/searchcal/

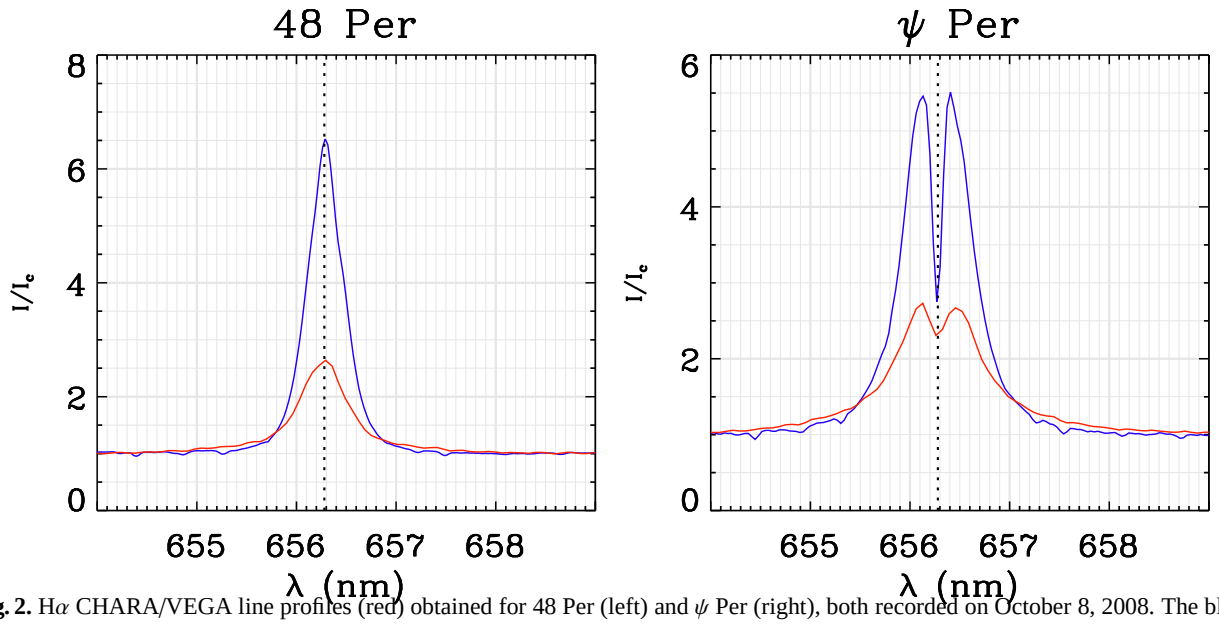

Fig. 2. Hα CHARA/VEGA line profiles (red) obtained for 48 Per (left) and ψ Per (right), both recorded on October 8, 2008. The blue lines are amateur spectra obtained from the BeSS database, recorded on October 10, 2008 for ψ Per, and on December 8, 2008 for 48 Per

moduli of the measured visibilities and the respective dates are given in Table 2.

Table 2. Visibility measurements, $V_{H\alpha}$, in the Hα line with spectral bandwidth $\delta\lambda$.

Star	Date (CTU)	$\delta\lambda$ (nm)	$V_{H\alpha}$
ψ Per	2008/10/07 11h33	2.4	0.49±0.03
	2008/10/08 06h52	2.4	0.66±0.04
	2008/10/09 07h48	2.4	0.32±0.11
	2008/10/09 10h43	2.4	0.37±0.15
48 Per	2008/10/07 12h48	1.75	0.57±0.04
	2008/10/08 07h29	1.75	0.65±0.03
	2008/10/09 07h03	1.75	0.35±0.13

The visibilities in the continuum near the Hα line of ψ Per and 48 Per were measured using the pass bands that are indicated in Table 3. Both visibilities in the Hα line and in the continuum were obtained using the spectral density mode (see sect. 3.2)

3.3. Spectral analysis

The *Hα* calibrated spectra that were extracted from our interferometric measurements are plotted in Fig 2. They have very different shapes: ψ Per is double-peaked, while 48 Per is single. Both line profiles reflect the different projections of the circuemstellar disks: it is nearly edge-on for ψ Per and at an intermediate inclination angle close to the pole-on for 48 Per. All Hα profiles exhibit large wings whose correspond to velocities on the order of 1000 km s^{-1} for the Doppler shifts. However, as we shall see in the following sections, they probably the result of other to physical processes than mere kinematic broadening.

Table 3. Visibility measurements in the continuum close to Hα and Hβ lines, along with the spectral bandwidths ($\delta\lambda$) used to obtain the visibilities with sufficient S/N.

Star	Date (CTU)	$\lambda_{central}$ (nm)	$\delta\lambda$ (nm)	V^2_{cont}
ψ Per	2008/10/07 11h33	639.0	22.0	0.78 ± 0.03
		667.0	12.0	0.79 ± 0.05
		497.25	7.5	0.69 ± 0.09
	2008/10/08 06h52	640.0	20.0	0.83 ± 0.02
		666.5	13.0	0.84 ± 0.03
		480.9	5.2	0.59 ± 0.09
		497.00	8.0	0.61 ± 0.14
	2008/10/09 07h48	637.5	25.0	0.65 ± 0.02
		497.1	7.45	0.82 ± 0.29
	2008/10/09 10h43	637.5	25.0	0.58 ± 0.08
		497.3	8.0	0.4 ± 0.08
		507.55	8.1	0.48 ± 0.13
48 Per	2008/10/07 12h48	641.0	18.0	0.84 ± 0.03
		666.0	12.0	0.85 ± 0.02
	2008/10/08 07h29	640.0	20.0	0.83 ± 0.02
		666.0	14.0	0.82 ± 0.03
		496.7	8.1	0.86 ± 0.1
	2008/10/09 07h03	496.3	6.6	0.73 ± 0.07
	2008/10/09 11h22	506.5	6.5	0.69 ± 0.05

Table 4. Comparison of the Hα equivalent width (EW) from CHARA/VEGA measurements and other spectroscopic data.

Star	Hα EW (Å)		Average Ratio	m_v
	VEGA	Spectro.		
ψ Per	19.9/22.4/24.7/22.1	40.8/37.3	1.75	4.23
48 Per	12.3/11.8/13.7/12.1	25.5/32.2	2.31	4.04

The Hα spectra taken from the BeSS database[2] are also plotted in Fig 2. These line profiles were recorded on October

[2] http://basebe.obspm.fr

Table 5. Hα EW, differential visibility and amplitude of phase variations obtained for γ Cas using different neutral density filters.

Neutral Density Filter	0.0	0.3	0.6
Hα EW (Å)	11.7	14.9	15.8
Diff. Vis. Amplitude (± 0.1)	0.6	0.7	0.6
Phase Amplitude (± 2°)	45	49	48

10, 2008 for ψ Per and on December 8, 2008 for 48 Per, while the Hα VEGA/CHARA line profiles (Fig 2) were recorded on October 8, 2008. We chose BeSS line profiles that are as close as possible to the epoch of our observations, so that they are expected be similar to their interferometric counterpart, both in terms of global intensity and in morphology, when reduced to the same spectral resolution.

In Table 4 we compare the equivalent widths (EW) of the lines measured from the BeSS database and those obtained in our interferometric measurements. We prefer to use the EW estimate instead of the line intensities to avoid differences induced by the rapidly varying asymmetric double-peaked line emission profiles. We found that for both objects the VEGA/CHARA red detector seems to underestimate the line flux by a factor 2-3. This is probably due to a saturation phenomenon that correlates with the magnitude of the object, but not with the line intensity. It is that not a local effect that affects the detector, but only the photon-counting algorithm. Accordingly, the measured visibilities and phase signals are not affected by this phenomenon.

To test this hypothesis, we recorded three datasets with different density filters: 0.0, 0.3, and 0.6 of another well known Be star: γ Cas. This star was observed on November 17, 2009 in the high spectral resolution mode centered on the H_α line, but since these measurements were done only for technical purposes, without any calibrator. As expected, due to the saturation effect, the line intensity was correlated with the density of the neutral filter. However, the visibility and phase variations were not affected. This is demonstrated in Table 5 where the line EW, visibility, and phase amplitude are given for each filter used. The given quantities clearly show that we do not need to correct the visibility and phase for line saturation effect. This is, nevertheless, not so for the VEGA/CHARA line profiles, which thus cannot be used directly for modeling.

4. DisK geometry from the Hα line and continuum spectrum analysis

4.1. Extent of the Hα line-emission region

The first step in the geometrical interpretation of the interferometric measurements is made by considering the Hα emitting region as a uniform or a Gaussian elongated disk. Unlike attempts previously made by several authors [c.f. Tycner et al (2005,2006)], where the free parameters characterizing the stellar and circumstellar environments are determined by interpreting the total observed visibility of the star+environment system, here we determined the free parameters that correspond to the circumstellar environment alone.

To do that, we assume that the total emitted flux in the Hα line has two components: one of them from the photospheric absorption of the star that underlies the circumstellar disc or envelope and the other corresponding to the emission produced in the circumstellar environment. For this simple model, we can write the expression of the modulus of the visibility measured in the Hα line as

$$V_{\mathrm{H}\alpha} = \frac{V_{\star\mathrm{H}\alpha} F_{\star\mathrm{H}\alpha} + V_{\mathrm{emH}\alpha} F_{\mathrm{emH}\alpha}}{F_{\mathrm{tot}}}, \quad (1)$$

where $V_{\star\mathrm{H}\alpha}$ and $F_{\star\mathrm{H}\alpha}$ are the visibility and the flux of the photospheric Hα absorption, while $V_{\mathrm{emH}\alpha}$ and $F_{\mathrm{emH}\alpha}$ are the visibility and the flux of the envelope in the Hα line. The F_{tot} flux is simply

$$F_{\mathrm{tot}} = F_{\star\mathrm{H}\alpha} + F_{\mathrm{emH}\alpha}. \quad (2)$$

The quantity of interest in our analysis of the emitting region ($V_{\mathrm{emH}\alpha}$) can then be written by using Eqs. 1 and 2:

$$V_{\mathrm{emH}\alpha} = \frac{V_{\mathrm{H}\alpha} - V_{\star\mathrm{H}\alpha} \frac{F_{\star\mathrm{H}\alpha}}{F_{\mathrm{tot}}}}{1 - \frac{F_{\star\mathrm{H}\alpha}}{F_{\mathrm{tot}}}}. \quad (3)$$

We now calculate the visibility of the photospheric absorption component from an estimate of the photospheric angular diameter. To estimate the ratio $\frac{F_{\star\mathrm{H}\alpha}}{F_{\mathrm{tot}}}$, we need to have an estimate of the Hα absorption profile. For that we use spectra of stars with similar spectral type and $V \sin i$ to that of the program object. For ψ Per we use HD 196740 and for 48 Per we use HD 87015 with both spectra are taken from the ELODIE/OHP spectrograph archives [3]. The Hα emission line profile of ψ Per adopted in this work was observed at times close to the dates of interferometric observations, on October 10, 2008, and it was taken from the "Spectroscopic Be star Atlas" [4]. On short time scales, the maximum emission intensity in this star varies by $\Delta I_{\mathrm{max}}/I_o \simeq 0.5$ around an average of $\langle I_{\mathrm{max}}/I_o \rangle = 5.6$. The adopted profile of the Hα emission line of 48 Per is from the "Be Star Spectra database" [5], taken on the December 12, 2008, the closest date of the interferometric observations that we could find in the literature. The maximum emission intensity in the Hα line of this star varies in $\Delta I_{\mathrm{max}}/I_o \simeq 0.7$ around a mean maximum intensity $I_{\mathrm{max}}/I_o = 6.3$.

The ratio $\frac{F_{\star\mathrm{H}\alpha}}{F_{\mathrm{tot}}}$ needed in Eq. 3 can then be estimated as

$$\frac{F_{\star\mathrm{H}\alpha}}{F_{\mathrm{tot}}} = \frac{1}{1 + F_{\mathrm{emH}\alpha}/F_{\star\mathrm{H}\alpha}}. \quad (4)$$

The flux ratio $F_{\mathrm{emH}\alpha}/F_{\star\mathrm{H}\alpha}$ can be derived using the above observed Hα line emission and absorption profiles, but only if we assume that the emission/absorption in the continuum spectrum due to the circumstellar envelope is negligible. We see in the next section that this contribution amounts to some 10% in both of the studied Be stars. With that assumption, the quantities $F_{\mathrm{emH}\alpha}/F_{\mathrm{tot}}$ and $F_{\star\mathrm{H}\alpha}/F_{\mathrm{tot}}$ could be calculated, and the results are given in Table 7.

[3] http://atlas.obs-hp.fr/elodie/

[4] http://astrosurf.com/buil/us/bestar.htm

[5] http://basebe.obspm.fr/basebe/

Best model results	Uniform disk model ψ Per	Uniform disk model 48 Per	Gaussian disk model ψ Per	Gaussian disk model 48 Per
Position Angle (in degree)	95 ± 2	110 ± 19	96 ± 2	115 ± 33
Elongation ratio	2.9	1.3	2.9	1.3
Minor axis (in mas)	2.19 ± 0.09	2.60 ± 0.14	1.38 ± 0.06	1.6 ± 0.15
Major axis (in mas)	6.4 ± 0.3	3.4 ± 0.2	4.0 ± 0.2	2.1 ± 0.2
Major axis (in $R_\star$)	17 ± 1	14 ± 1	11 ± 0.6	8 ± 0.76
χ^2_{red}	0.51	0.56	0.52	0.62

Table 6. Best parameters obtained with `LITpro` for ψ Per and 48 Per for two models in the Hα line. These parameters were obtained for an inclinaison angle of 70° (i.e Elongation ratio = 2.9) and 39° (i.e Elongation ratio = 1.3) for ψ Per and 48 Per respectively, which where the inclination angles that produce the smallest reduced χ^2.

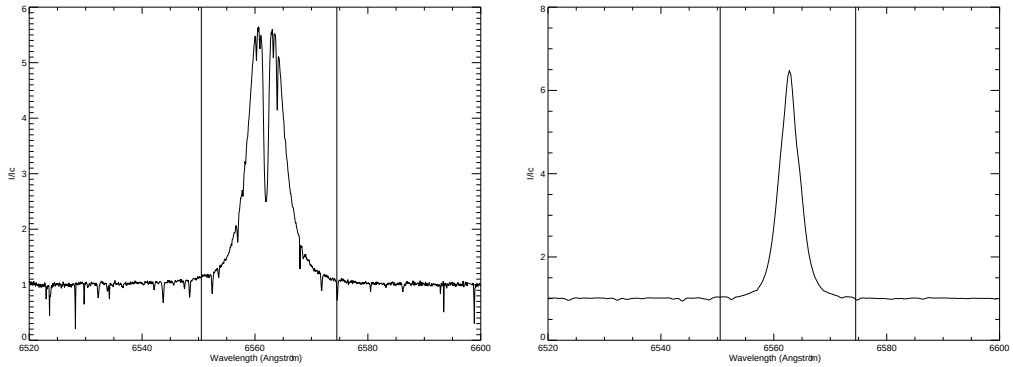

Fig. 3. Spectral bandpass used to compute normalized flux in the H_α line of each component for ψ Per (left) and 48 Per (right) (see Table 7)

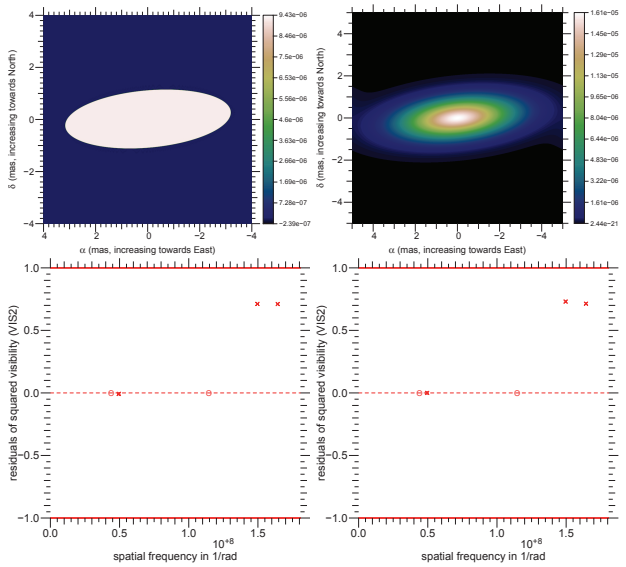

Fig. 4. Best model for ψ Per disk obtained with the `LITpro` software in the Hα line. On top, uniform (left) and Gaussian (right) 2D map of the disk projected onto the skyplane. East is to the left. On bottom, residual visibilities for ψ Per for the uniform disk model (left) and the Gaussian disk model (right) in the Hα line. Y axes are given in standard deviation σ

The adopted 'photospheric' angular diameters are taken from Quirrenbach et al. (1997): 0.35 mas for ψ Per and 0.34 mas for 48 Per. We can now interpret the emitting region as caused by an apparent elliptical disks that have either a uniform or a Gaussian brightness distribution. Three free parameters are needed for that: when disks are interpreted as having uniform brightness, the parameters to determine are the angular diameter of the minor axis of the apparent elliptical disk $\theta_{\rm m}$, the ratio of the major to the minor axis of the elliptical disk $r = R_{\rm M}/R_{\rm m}$ (also called the elongation ratio), and the position angle of the major axis position angle measured eastward from the north. By using a Gaussian distribution of the disk brightness, we have the same free parameters, except that the size

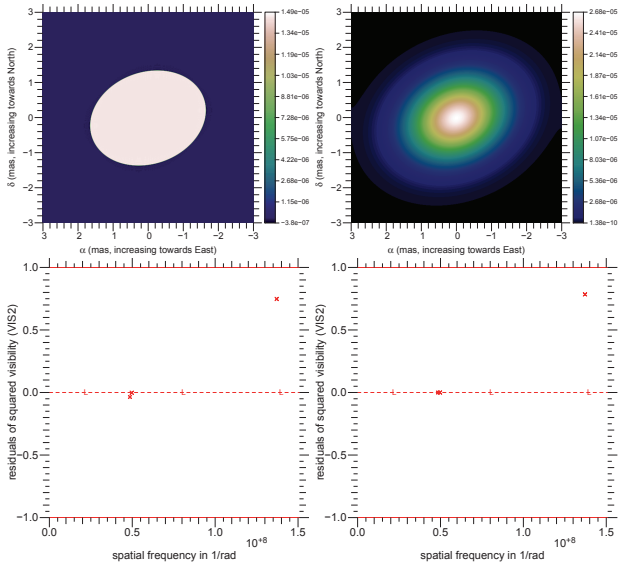

Fig. 5. Best model for 48 Per disk obtained with the `LITpro` software in the Hα line

Table 7. Normalized flux in the H_α line of each component for ψ Per and 48 Per.

	ψ Per	48 Per
$\frac{F_{\rm emH\alpha}}{F_{\rm tot}}$	0.825	0.844
$\frac{F_{\star \rm H\alpha}}{F_{\rm tot}}$	0.175	0.156
Bandpass	2.4 nm	1.7 nm

of the minor axis is replaced by the FWHM of the minor axis component of the brightness distribution.

The free parameters were determined with the LITpro program developed by the JMMC working team (Tallon-Bosc et al. 2008). This program takes the characteristics of each interferometric configuration into account and explores the whole space of parameters to find the quantities $\theta_{\rm M}$, r and position angle of the major axis of the disk. Finally, if we assume that the circumstellar environments are flat disks, their apparent elliptical shape leads to an estimate of the respective inclination angles i:

$$i = \arccos(1/r). \quad (5)$$

Because of the lack of available data, the elongation ratio r was estimated step by step. So, to determine r, we ran the LITPro software for different fixed values of r. Finally, we selected the r value that produces the smallest χ^2. The parameters of the circumstellar disks of ψ Per and 48 Per are given in Table 6. Figures. 4 and 5 show the projected intensity maps that correspond to the best set of parameters calculated for each adopted model of the brightness distribution in the circumstellar disks and residual visibility plots for each model. In this last plot, Y axes are given in standard deviation σ.

4.2. Disc extent from the continuum

In contrast to the analysis done with the Hα emission line, where we could separate the stellar and the envelope contributions to the observed line profile, we cannot do the same in the case of the continuum spectrum. This would only be possible if we could catch the stars at phases with and without circumstellar emission. As in (1) for the Hα emission line, we write the visibility for the continuum spectrum as

$$\begin{aligned} V_{\rm cont} &= \frac{V_{\star \rm cont} F_{\star \rm cont} + V_{\rm env\_cont} F_{\rm env\_cont}}{F_{\rm tot\_cont}} \\ F_{\rm tot\_cont} &= F_{\star \rm cont} + F_{\rm env\_cont}, \end{aligned} \quad (6)$$

Table 8. Parameters obtained for the circumstellar gaussian discs of ψ Per and 48 Per contributing to the continuum spectrum

	ψ Per	48 Per
$\theta_{\rm UD\star}$ (in mas)	0.37 ± 0.04	0.25 ± 0.05
$F_{\star \rm cont}/F_{\rm tot\_cont}$	0.88 ± 0.16	0.9
$F_{\rm env\_cont}/F_{\rm tot\_cont}$	0.12 ± 0.03	0.1
$\theta_{\rm m\_cont}$ (in mas)	2.00 ± 0.28	2.69 ± 0.28
Flattening ratio $r_{\rm c}$	2.9 (Hα model)	1.3 (Hα model)
PA of major axis	96 ° (Hα model)	110 ° (Hα model)
Reduced χ^2	0.76	0.37
$\theta_{\rm M\_cont}$ (in mas)	5.8 ± 1.6	3.5 ± 0.4
$R_{\rm M\_cont}$ (in $R_\star$)	15 ± 4	14 ± 1.6

where $V_{\rm cont}$ is the measured visibility modulus in a given spectral pass band, $V_{\star \rm cont}$ and $F_{\star \rm cont}$ are the visibility modulus and the continuum flux of the star, and $V_{\rm env\_cont}$ and $F_{\rm env\_cont}$ are the visibility modulus and the continuum flux due to the circumstellar envelope. Either the flux ratio $F_{\star \rm cont}/F_{\rm tot\_cont}$ or $F_{\rm env\_cont}/F_{\rm tot\_cont}$ can now be treated as a free parameter.

The observed visibility modulus (6) is interpreted as due to a central star with a uniform disk brightness and a circumstellar disc modeled with a Gaussian brightness distribution having an apparent elliptical shape. This model has five free

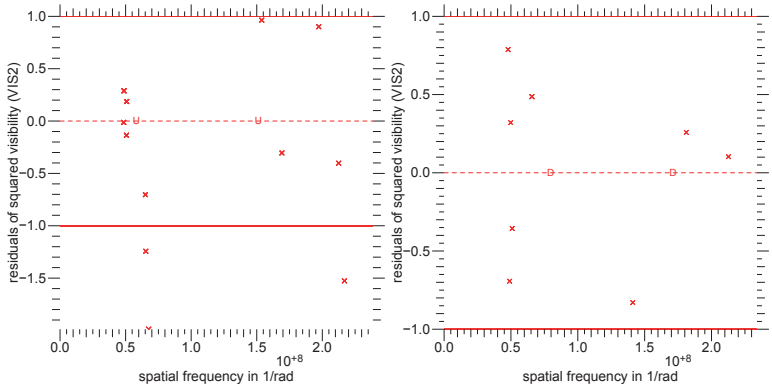

Fig. 6. Residual plot for our best model for ψ Per (left) and 48 Per (right) in the continuum.

parameters: the stellar angular diameter $\theta_{\rm UD\star}$;,the angular diameter of the minor axis of the Gaussian disk contributing to the continuum flux $\theta_{\rm m\_cont}$, the normalized stellar continuum flux $F_{\star\rm cont}/F_{\rm tot\_cont}$, the ratio of the major to the minor axis of the elliptical disk emitting in the continuum (flattening ratio) $r_{\rm c} = R_{\rm M\_cont}/R_{\rm m\_cont}$, and the position angle of the major axis of the elliptical disk position angle measured eastward from the north. The free parameters were calculated as before using the LITpro software. In this analysis we made two assumptions: that the elongation of the continuum emitting zone is the same as for the Hα line emission and that the position angle derived previously with the Hα emission line is also the same for the continuum. Because there is not enough data for 48 Per at our disposal, we also preferred to fit the flux ratio $F_{\star\rm cont}/F_{\rm tot\_cont}$ in this star and adopt the value that produces the best χ^2. The quantities that characterize the circumstellar region contributing to the emitted continuum spectrum in the program stars obtained are summarized in Table 8, and residual visibilities are plotted in Fig. 6 .

Taking the roughly 20% uncertainties affecting the Barnes-Evans method into account, we note that our results concerning the stellar angular diameters derived from the continuum spectrum are in good agreement with those reported by Quirrenbach et al. (1997), i.e. 0.33 mas for ψ Per and 0.34 mas for 48 Per. Regarding the angular diameters of the circumstellar continuum emitting regions, our estimate for ψ Per is twice as large as in Quirrenbach et al. (1997), while for 48 Per it is very close to the value obtained by these authors (2.77±0.56 mas). However, these comparisons can be misleading, since the emission in Be stars is known to be fairly variable.

Finally, we stress that our W1W2 projected baseline of 108.8 m enabled us to resolve the central star of 48 Per, while Quirrenbach et al. (1997) probably could not resolve it with the 31.5 m baseline of the MkIII.

5. Modeling the circumstellar envelope

5.1. Data in the differential analysis mode

Data for 48 Per and ψ Per using the cross-spectral density analysis mode are presented in Fig. 7. For each star, we have plotted the visibility and the differential phase as a function of wavelength around the Hα line. The visibility curves clearly indicate that the Hα region is partially resolved; that is, the visibility is less than 1.0, with the shortest baselines and fully resolved with the longest baselines. We also notice the large broadening in the wings of the visibility curves. Two hypothesis will be discussed in Sect. 5.3 to explain this effect. We see that the differential phase plots exhibit "S" shapes, which are clear signatures for rotating disks (Meilland et al. 2007b). The absence of this "S" shape for the B_2 baseline observation of 48 Per perhaps comes from the B_2 baseline being oriented close to the direction of the stellar rotational axis so that no photocenter displacement, which produces a fringe phase shift, is expected in this direction. Finally, let us note the complex behavior of the differential phase for the largest baselines. This is most probably because the disk is fully resolved. There is a direct relation between photocenter displacements and fringe phase shifts, but this is only a first-order effect when the object is unresolved or barely resolved. Observations on the larger baselines are sensitive to small-scale features on the disk itself, which are neither considered nor reproduced by our simple kinematic disk model presented in the next section.

5.2. The kinematic disk model

To constrain the kinematics in the circumstellar environment of both stars, we have used a simple model that was developed in order to allow fast fitting of observations concerning rotating and/or expanding geometrically thin disks around stars. For the rotation velocity the model adopts a simple power law:

$$V_\phi = V_{\rm rot}\left(\frac{r}{R_\star}\right)^\beta \tag{7}$$

where $V_{\rm rot}$ is the stellar rotational velocity and r the distance to the center of the star. In this model $\beta = -0.5$ corresponds to Keplerian rotation, and $V_{\rm rot}$ can be considered proportional or equal to the stellar critical velocity $V_{\rm c} = \sqrt{2GM_\star/3R_{\rm p}}$, where $M_\star$ is the stellar mass and $R_{\rm p}$ its polar radius. The expansion velocity is assumed to be given by a CAK wind model (Castor et al. 1975):

$$V_{\rm r} = V_0 + (V_\infty - V_0)\left(1 - \frac{R_\star}{r}\right)^\gamma \tag{8}$$

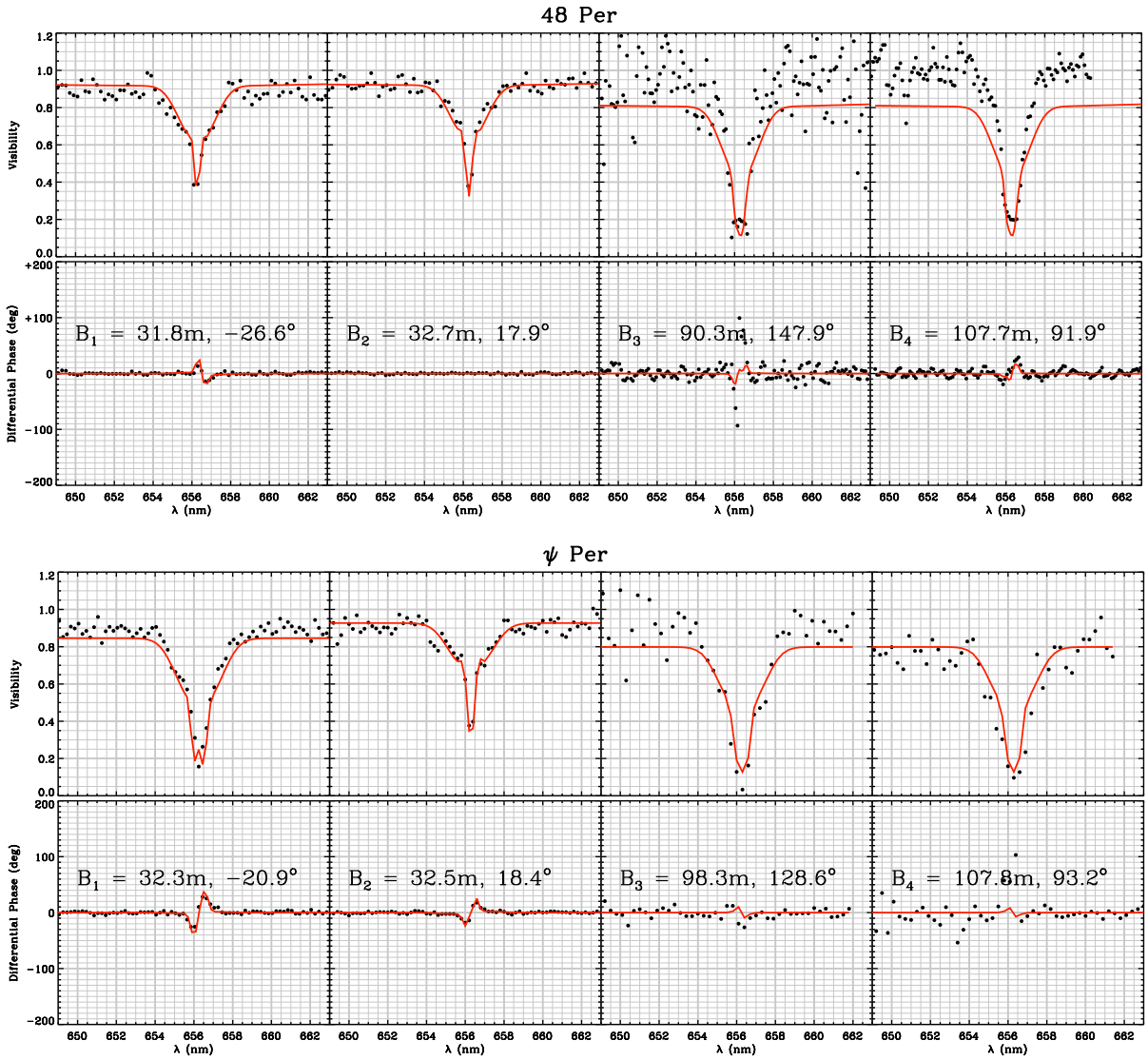

Fig. 7. Calibrated measurements for 48 Per & ψ Per: visibility (upper line) and differential phase (lower line) for different baseline lengths and the projected angles indicated for each plot. The visibility and phase from our best-fit models for 48 Per and ψ Per are overplotted in red (plain line).

where V_0 is the expansion velocity at the photosphere and V_∞, the terminal expansion velocity. For typical wind models of hot stars $\gamma = 0.86$. Both velocity fields (7) and (8) are then combined and projected along the line of sight, taking into account the inclination angle i of the star-disk system resulting in

$$V_{\rm proj}(x,y) = \left(V_\phi \sin\phi - V_{\rm r}\cos\phi\right) \times \sin i \qquad (9)$$

where x and y are the spatial Cartesian coordinates on the sky plane. To compute two-dimensional iso-velocity maps within an emission line projected onto the sky-plane, we compute for each spectral channel $\delta\lambda$ the map of pixels that correspond to the iso-velocity region defined by $\delta\lambda$ according to:

$$R(x,y,\lambda,\delta\lambda) \;=\; \frac{1}{\sigma\sqrt{2\pi}}\exp\left[-\left(\frac{V_{\rm proj}(x,y)-V(\lambda)}{\sqrt{2}\sigma}\right)^2\right]$$

$$\sigma \;=\; \frac{\delta V}{2\sqrt{2\,ln(2)}} = \frac{\delta\lambda\, c}{2\lambda\sqrt{2\,ln(2)}} \qquad (10)$$

where $V(\lambda)$ is the Doppler displacement corresponding to λ in the line profile.

We model the intensity distribution of the spectral line projected onto the sky plane as a normalized flattened Gaussian distribution I_{line}(x,y). The flattening is due to the projection on the sky plane of the geometrically thin disk; i.e., f = 1/cos(i). To build the intensity map at each wavelength (λ) and within narrow spectral bands ($\delta\lambda$), we multiply each iso-velocity map R(x,y,λ,$\delta\lambda$) by I_{line}(x,y). The spectrally-resolved intenisity maps are finally normalized by the total line equivalent width (EW).

We model the central star as a uniform disk with a constant brightness $I_\star$(x,y) while the continuum emitted by the circumstellar disk I_{env}(x,y) is modeled by a flattened Gaussian distri-

bution with the same flattening as $I_{line}(x,y)$. As for $I_{line}(x,y)$, $I_\star(x,y)$ and $I_{\rm env}(x,y)$ are normalized by their respective total flux. The envelope flux in the continuum F_{env} is constant, while the relative flux of the central star $F_\star$ to the total flux is a function of wavelength to be able to consider photospheric line and/or strong absorption features such as shell lines.

Finally, we obtain the total emission maps for each spectral channel by adding the three contributions with their relative fluxes:

$$I_{\rm tot}(x,y,\lambda,\delta\lambda) = I_\star(x,y)\times F_\star(\lambda) + I_{\rm env}(x,y)\times F_{\rm env} + I_{\rm line}(x,y)\times R(x,y,\lambda,\delta\lambda)\times {\rm EW}. \quad (11)$$

This simple model enables us to calculate a $256\times256\times100$ data cube corresponding to 256×256 pixels of the map and 100 different wavelengths in the line and nearby continuum. This calculation takes less than one second on a "standard" computer. The computed maps can then be rotated to fit the observational position angle and/or scaled using the stellar radius $R_\star$ and distance d. The wavelength dependent visibilities and phases for several baselines can then be calculated using standard Fourier transform methods. The total computing time for one simulated interferometric dataset is a few seconds to allow us to perform automatic model fitting as for instance with the Levenberg-Marquart method. However, this procedure involves calculation of some 10 free parameters, whose determination may in some cases be somewhat longze.

5.3. Line wing broadening

After having computed hundreds of models we were not able to reproduce all of the observed data. It was not possible to simultaneously fit the large wings in the visibility, the intensity profile that would correspond to more than 1000 kms^{-1} of Doppler displacement, and the narrower differential phase variations of a few hundred km s^{-1}. Despite the poor fits of the line wings, we did manage to simultaneously fit the central part of the line intensity, both the visibility and the differential phase, with a pure rotating disk model having a smaller stellar radii, where the major-axis is oriented perpendicularly to the polarization angle in ψ Per and parallel to it for 48 Per. In what follows we explore some hypotheses that could in principle explain the origin of these wide spread wings.

The polar wind hypothesis: In this hypothesis we consider a quickly expanding spherical stellar wind. Since the polar terminal wind velocities in Be stars determined from fra-UV lines are in the range 1000-2000 kms^{-1}, they are compatible with the Doppler displacements of the emission line wings. Nevertheless, it is unlikely that polar winds contribute significantly to the emission in the Hα line, as the density in the polar wind is by some orders of magnitude lower than in the equatorial plane. Kervella & Domiciano de Souza (2007) and Meilland et al. (2007b) measured polar wind contributions and found that they are only a few percent of the total near-infrared flux in the Be stars Achernar and α Arae. However, these winds were not spherical and they would create a differential phase signal in the line. Moreover, this hypothesis cannot explain the line broadening in ψ Per, which is a Be-shell star likely seen edge-on. Consequently, the projected polar wind velocity cannot produce components in the line of sight large enough to account for the measured broadening up to some 10^3 km s^{-1}.

Keplerian shear hypothesis: The Keplerian shear provides significant Doppler gradients thereby enabling the photons trapped in optically thick layers to escape easily from the circumstellar envelopes and produce significantly enlarged wings in emission lines (Horne & Marsh 1986). The Doppler width of an intrinsic Gaussian line profile can be enlarged by a "turbulent-like" term due to the differential rotation in the disk projected towards the observer. For circumstellar media optically thick enough wide P Cyg line profiles can be produced, but also bottle-like line shapes with line wings that are broader for the higher the inclination angles. The same shear can also produce extremely large absorption wings. These effects were studied by Arias et al. (2007).

The incoherent scattering hypothesis: A non-coherent scattering redistribution is one where the frequency of radiation re-emitted within the lines does not depend only on the radiation absorbed in the same frequency. Discussions of the consequences of this incoherent redistribution in the formation of absorption line wings date back to Spitzer (1944) and Münch (1949). More systematic accounts on this process can be found in Mihalas (1978). The influence of the incoherent electron scattering on the emission line formation in Wolf-Rayet stars was studied by Castor et al. (1970). The combination of kinematics, incoherent scattering and non-LTE effects on the source function of Balmer lines in circumstellar envelopes, can produce broadened wine-bottle-like line profiles with extended wings (Hummel & Dachs 1992).

In this work we decided to explore only this last effect as explained in the next section.

5.4. Emission line broadening by incoherent scattering

The line broadening by incoherent scattering in the Hα emission line is estimated here by introducing two parameters to our kinematic-model: the global ratio of the scattered photons and the spectral width of the scattering. This ad-hoc treatment of the phenomenon is certainly a major caveat in our approach. Better calculations of this effect can be performed by using recent models, such as the non-LTE radiative transfer *BEDISK* code developed by Sigut & Jones (2007).

For both objects we have taken the Hα photospheric line underlying the circumstellar emission line into account. For this, we used the photospheric line profiles obtained using a SYNSPEC model (Hubeny 1988; Hubeny & Lanz 1995), broadened by the corresponding rotational velocity. In the case of objects seen at high inclination angles one has to also consider the absorption of the stellar radiation by the circumstellar disk itself. Whenever the disk opacity in the lines is high enough, a deep-narrow absorption appears at the center of emission lines. The resulting double-peaked emission lines with a narrow absorption at its center are called "Be-shell" line profiles. ψ Per exhibits such line profiles, and is therefore ex-

Table 9. Best-fit kinematic-model parameters for 48 Per and ψ Per, with the position angle of the major axis.

	Disk geometry in the continuum				Disk geometry in the line		Disk kinematics		non-coherent scattering	
Star	FWHM$_c$ (R$_\star$)	i (°)	P.A. (°)	F$_{env}$	EW$_l$ (Å)	FWHM$_l$ (R$_\star$)	V$_{rot}$ (km s^{-1})	β (Eq. 6)	Width (Å)	Ratio
ψ Per	15±5	75±8	115±20	0.15±0.05	43±4	20±4	400±20	-0.35±0.05	20±6	0.4±0.1
48 Per	9±2	30±10	108±1	0.1±0.05	36±3	9±1	440±30	-0.5±0.1	18±4	0.4±0.1

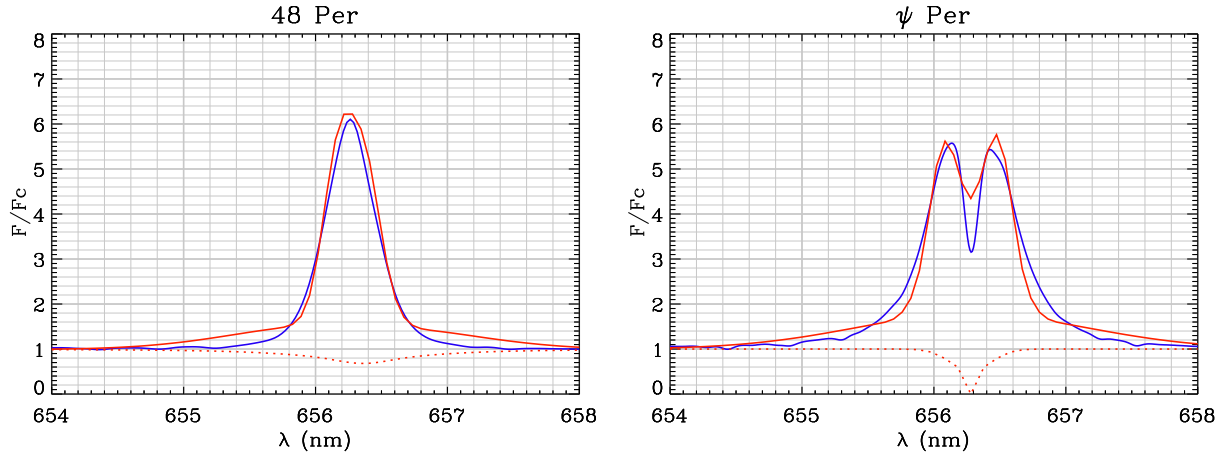

Fig. 8. 48 Per (right) and ψ Per (left) fit of the Hα line profiles. red dotted line: Simulated stellar absorption line, including shell absorption for ψ Per. Blue line: BeSS spectrum convolved with CHARA/VEGA spectral-resolution. Red solid line: line computed from the best-fit kinematic model. Note the good agreement at the center of the line, whereas our model produces line wings too large compared to the amateur spectrum.

pected to have a high inclination angle. To include this phenomena in our model, we modified the relative stellar flux F$_\star(\lambda)$, by adding a strong and narrow absorption at the center of the Hα line.

Previous spectrally resolved interferometric observations (Meilland et al. 2007a,b) and spectroscopic follow-ups (Miroshnichenko et al. 2003; Vinicius et al. 2006) showed evidence that the kinematics in the equatorial plan was dominated by rotation. Thus, because of the lack of available measurements for our targets and the introduction of additional parameters needed to take into account the incoherent scattering effect, we decided to neglect the expansion in the equatorial disk (i.e., $V_0 = V_\infty = 0$ kms^{-1}).

We ran several hundred models for each target to probe the parameter space. The visibility and phase for the best-fit models for 48 Per and ψ Per are overplotted in Fig. 7, and the fits of the Hα spectra are plotted in Fig 8. The corresponding parameter values of the kinematic model are given in Table 9. Errors on the parameters are only "local" estimates based on the measured errors on the visibility and phase. The uniqueness of the best-fitted models are not clearly established because the effect of many parameters on the visibility and phase are not fully independent. Consequently, these models have to be considered as "best" models but not unique ones. We note, however, that the agreement between the model and observed differential phases is better for the short baselines (B_1 and B_2) than for the longer ones (B_3 and B_4). This is mainly because the circumstellar disk is resolved at the longest baselines, so that the phase variations are dominated by a smaller structure, and our model does not take this behavior into account. We also note that while we obtain good agreement at the center of the line, our model produces line wings that are too broad for the observed spectrum, but close to the interferometric ones. This is probably due to our add-hoc way of modeling the incoherent scattering so it is discussed in the next section.

6. Discussion

6.1. Comparison of the disk extensions between the LITpro and the kinematic models

In Figs. 3 and 4, we present the maps of ψ Per and 48 Per disk that we obtained with the LITpro Software in the whole Hα line. We used two models to fit our data: a uniform and a Gaussian disk model. The free parameters for these two models are the minor axis, the position angle, and the flattening ratio of the disk, but we can also choose to fix one parameter and let the other two remain free. For our purpose, and due to the limited measurements we obtained, we fixed the flattening ratio, knowing the inclination angle of the disk, which was previously derived from the simple kinematic disk model used to interpret the differential phases (see previous section). For both models we obtained a small reduced χ^2 (see Table 6), but we were not able to clearly differentiate the two models. If we compare the LITpro models and the kinematics disk model (see Table 9), we obtain good agreement for 48 Per for the Gaussian disk model (see the right part of Table 6), whereas for ψ Per, the LITpro model provides a disk extension that is somehow smaller than the one obtained with the kinematic disk model.

6.2. Disk orientation and polarization measurements

Quirrenbach et al. (1997) estimate a minimum inclination of $i = 62^\circ$ for ψ Per and $i = 27^\circ$ for 48 Per from a fit of an ellipsoidal Gaussian and clearly explain that they cannot determine this inclination directly from their observations. From our simple kinematic model we obtain respectively $i = 75 \pm 8^\circ$ and $i = 30 \pm 10^\circ$, in agreement with the LITpro fit in the whole H_α line but with a stronger constraint since the differential phase and the shape of the emission line profile are very sensitive to this inclination angle.

With these inclination angles, we obtain a position angle for the disk major axis of $115 \pm 20^\circ$ and $108 \pm 1^\circ$ for ψ Per and 48 Per, which again agree with our independent fit within the whole Hα line with the LITpro code. Yudin (2001) obtain a polarization of 0.17% for 48 Per and a position angle for the major axis of 110°. This position angle is very close to our measurement of 108° for the major axis position, thus the polarization seems to be parallel to the disk, which is quite unusual for a Be star. The polarization position angle in an optically thin axisymmetric disk is usually perpendicular to the plane of the disk since it mainly comes from electron scattering (Brown & McLean 1977). On the other had, if the polar regions of the envelope, i.e. a polar stellar wind as already observed for α Arae and Achernar, are dense enough, they can dominate the polarization and the polarization position angle will be parallel to the plane of the disk (Wood et al. 1996). Since 48 Per is supposed to be seen close to the polar regions ($i = 30 \pm 10^\circ$ from our spectrally resolved measurements), we may in fact be detecting an extended stellar wind rather than an equatorial disk.

The situation is clearer for ψ Per, where we obtained a major-axis position angle of $115 \pm 20^\circ$, whereas the polarization position angle determined by Yudin (2001) is 35°, i.e., the polarization position angle is nearly perpendicular to the major axis of the disk. This is not a surprise since ψ Per is a strong Be-shell with an inclination angle $i = 75 \pm 8^\circ$, close to the edge-on case; thus, even if the equatorial optical depth is large enough to produce a shell-line profile, the polar wind, if present, is not dense enough to dominate the polarized light.

6.3. Disc kinematics and stars

The kinematics of both disks are compatible with pure, rotating models. In the case of 48 Per, the rotation is clearly Keplerian, with a rotational velocity at the photosphere of $440 \pm 20 \mathrm{kms}^{-1}$, thus compatible with the critical velocity of 397 ± 20 km s^{-1} determined by Frémat et al. (2005) and exponent $\beta = -0.5 \pm 0.05$ in the velocity law (7). For ψ Per, the rotational velocity at the photosphere is also compatible with the critical velocity i.e. 400 ± 20 km s^{-1} (compared to 386 ± 21 km s^{-1}), but $\beta = -0.35 \pm 0.50$ This would imply that the disk is rotating faster than Keplerian motion requires. Such a rotational exponent β in the rotation law (7) has already been obtained by Meilland et al. (2007a) for the Be star κ CMa, but κ CMa was rotating at only 52% of its critical velocity. However, we have to keep in mind that our simple geometrically thin model might not be fully suitable for stars seen under high inclinations.

It nevertheless appears that both stars are rotating close to their critical velocity. Consequently, we can assume that the main physical phenomena responsible for the mass ejection for these Be stars is the stellar rotation itself. This effect has recently studied by Cranmer (2005) who finds that, from a detailed statistical determination of the equatorial rotation rates of classical Be stars, rapid rotation is likely to be linked to the ejection of gas that forms the observed circumstellar disks. Interestingly, he also finds that below 18000 K the threshold ratio $V_{\mathrm{min}}/V_{\mathrm{crit}}$ (where V_{min} is the minimum equatorial velocity, and V_{crit} is the critical rotation speed) goes to unity as T_{eff} decreases towards the end of the B spectral class. Thus, it is relatively easy for these Be stars to form a Keplerian disk thanks to their proximity to critical rotation. This is clearly the case for ψ Per and 48 Per, two Be stars with a T_{eff} on the order of 16000 K, as obtained by Frémat et al. (2005).

7. Conclusion

We observed two very different Be stars: 48 Per, a nearly pole-on Be star, and ψ Per, a Be-shell star close to edge-on geometry. Both stars are found to be nearly critical rotators even if 48 Per seems to shelter a Keplerian rotating disk, whereas for ψ Per the rotation is found to be faster [with $\beta = -0.35$ in law (7)]. However, considering the limitations inherent in our simple model, this last fact must be taken with caution.

One other interesting result is that the major-axis of 48 Per is parallel to the polarization angle and not perpendicular to it, as already observed for many Be stars (i.e. including ψ Per). This might be due to the disk optical thickness, which is also responsible for the incoherent scattering of a non negligible part of the line emission. To our knowledge, this is the first time that this effect for a Be star has been seen.

Assuming a simple uniform disk model for the stellar photosphere for the continuum and a Gaussian distribution of the brightness in the whole line emission regions, we obtained a ratio of the disk diameter D_{disk} to the photospheric diameter $D_\star$ of ~ 8 and ~ 11 respectively for 48 Per and ψ Per, which are to be compared with the ratios 8.0 and 9.4 obtained by Quirrenbach et al. (1997). This agreement is somehow surprising since Quirrenbach et al. (1997) assumes a photospheric diameter from the Barnes-Evans relation, whereas our measurements include the contribution to the continuum of the envelope free-free and free-bound emission. The envelope of ψ Per appears to be 2 times more flattened than the one for 48 Per, which is not surprising since 48 Per is seen close to a pole-on inclination, whereas ψ Per is seen equator-on.

Acknowledgements. VEGA is a collaboration between CHARA and OCA/LAOG/CRAL/LESIA that has been supported by the French programs PNPS and ASHRA, by INSU, and by the Région PACA. The project has obviously benefited from the strong support of the OCA and CHARA technical teams. The CHARA Array is operated with support from the National Science Foundation through grant AST-0908253, the W. M. Keck Foundation, the NASA Exoplanet Science Institute, and from Georgia State University. This work made use of the BeSS database, operated at GEPI, Observatoire de Meudon, France: http://basebe.obspm.fr, use of the Jean-Marie Mariotti Center

SearchCal service [6] co-developed by FIZEAU and LAOG, and of CDS Astronomical Databases SIMBAD and VIZIER [7].This work also made use of the Jean-Marie Mariotti Center LITpro service co-developed by CRAL, LAOG, and FIZEAU. [8]

References

Arias, M. L., Zorec, J., Cidale, L., et al. 2006, A&A, 460, 821

Arias, M. L., Zorec, J., & Frémat, Y. 2007, in Astronomical Society of the Pacific Conference Series, Vol. 361, Active OB-Stars: Laboratories for Stellare and Circumstellar Physics, ed. A. T. Okazaki, S. P. Owocki, & S. Stefl, 419

Barnes, T. G. & Evans, D. S. 1976, MNRAS, 174, 489

Barnes, T. G., Evans, D. S., & Parsons, S. B. 1976, MNRAS, 174, 503

Bjorkman, J. E. & Carciofi, A. C. 2004, in Bulletin of the American Astronomical Society, Vol. 36, Bulletin of the American Astronomical Society, 773

Bonneau, D., Clausse, J., Delfosse, X., et al. 2006, A&A, 456, 789

Brown, J. C. & McLean, I. S. 1977, A&A, 57, 141

Burbidge, G. R. & Burbidge, E. M. 1953, ApJ, 117, 407

Campbell, W. W. 1895, ApJ, 2, 177

Castor, J. I., Abbott, D. C., & Klein, R. I. 1975, ApJ, 195, 157

Castor, J. I., Smith, L. F., & van Blerkom, D. 1970, ApJ, 159, 1119

Cranmer, S. R. 2005, ApJ, 634, 585

Dougherty, S. M. & Taylor, A. R. 1992, Nature, 359, 808

Frémat, Y., Zorec, J., Hubert, A., & Floquet, M. 2005, A&A, 440, 305

Gehrz, R. D., Hackwell, J. A., & Jones, T. W. 1974, ApJ, 191, 675

Grundstrom, E. D. & Gies, D. R. 2006, ApJ, 651, L53

Hanuschik, R. W. 1996, A&A, 308, 170

Horne, K. & Marsh, T. R. 1986, MNRAS, 218, 761

Hubeny, I. 1988, Computer Physics Communications, 52, 103

Hubeny, I. & Lanz, T. 1995, ApJ, 439, 875

Hummel, W. & Dachs, J. 1992, A&A, 262, L17

Kervella, P. & Domiciano de Souza, A. 2006, A&A, 453, 1059

Kervella, P. & Domiciano de Souza, A. 2007, A&A, 474, L49

Meilland, A., Millour, F., Stee, P., et al. 2007a, A&A, 464, 73

Meilland, A., Stee, P., Vannier, M., et al. 2007b, A&A, 464, 59

Mihalas, D. 1978, Stellar atmospheres /2nd edition/, ed. Mihalas, D.

Miroshnichenko, A. S., Bjorkman, K. S., Morrison, N. D., et al. 2003, A&A, 408, 305

Mourard, D., Clausse, J. M., Marcotto, A., et al. 2009, A&A, 508, 1073

Münch, G. 1949, ApJ, 109, 275

Poeckert, R. & Marlborough, J. M. 1978a, ApJ, 220, 940

Poeckert, R. & Marlborough, J. M. 1978b, ApJS, 38, 229

Quirrenbach, A., Bjorkman, K. S., Bjorkman, J. E., et al. 1997, ApJ, 479, 477

Rinehart, S. A., Houck, J. R., & Smith, J. D. 1999, AJ, 118, 2974

Ruusalepp, M. 1982, in IAU Symposium, Vol. 98, Be Stars, ed. M. Jaschek & H.-G. Groth, 303–310

Sigut, T. A. A. & Jones, C. E. 2007, ApJ, 668, 481

Slettebak, A. 1949, ApJ, 110, 498

Spitzer, Jr., L. 1944, ApJ, 99, 1

Stee, P. 2003, A&A, 403, 1023

Struve, O. 1931, ApJ, 73, 94

Taylor, A. R., Waters, L. B. F. M., Lamers, H. J. G. L. M., Persi, P., & Bjorkman, K. S. 1987, MNRAS, 228, 811

ten Brummelaar, T. A., McAlister, H. A., Ridgway, S. T., et al. 2005, ApJ, 628, 453

Tycner, C., Jones, C. E., Sigut, T. A. A., et al. 2008, ApJ, 689, 461

Underhill, A. B., Divan, L., Prevot-Burnichon, M., & Doazan, V. 1979, MNRAS, 189, 601

Vinicius, M. M. F., Zorec, J., Leister, N. V., & Levenhagen, R. S. 2006, A&A, 446, 643

Waters, L. B. F. M. 1986, A&A, 162, 121

Waters, L. B. F. M., Cote, J., & Lamers, H. J. G. L. M. 1987, A&A, 185, 206

Waters, L. B. F. M. & Marlborough, J. M. 1992, A&A, 256, 195

Wood, K., Bjorkman, J. E., Whitney, B., & Code, A. 1996, ApJ, 461, 847

Yudin, R. V. 2001, A&A, 368, 912

Zorec, J., Arias, M. L., Cidale, L., & Ringuelet, A. E. 2007, A&A, 470, 239

[6] Available at http://www.jmmc.fr/searchcal

[7] Available at http://cdsweb.u-strasbg.fr/

[8] LITpro softwar! e available at http://www.jmmc.fr/litpro